Direct numerical simulation of H-type and K-type transition to turbulence

By T. Sayadi, C. W. Hamman AND P. Moin

1. Motivation and objectives

Disturbances are introduced inside a laminar boundary layer by means of a receptivity process. This process is a response of the boundary layer to either external or internal perturbations. K-type and H-type transitions are two main transitional scenarios that lead to turbulence in an incompressible boundary layer. These transition scenarios belong to the class of controlled transitions. The receptivity process is controlled such that it leads to generation of the prescribed two- and three-dimensional waves with low amplitudes. These disturbances grow as predicted by linear stability theory and during this process no external or internal perturbations are allowed to interact with the boundary layer unlike the continuous perturbations applied to the near-wall boundary layer when strong free-stream disturbances are present.

In K-type transition (Klebanoff *et al.* 1962), the two-dimensional Tollmien-Schlichting (TS) wave interacts with a pair of oblique waves of lower amplitude and same frequency, which leads to the generation of aligned Λ-shaped vortices that precede arrow-shaped turbulent spots. These spots merge and the boundary layer ultimately becomes turbulent. In the H-type regime (Herbert 1988), the three-dimensional oblique waves have half the frequency of the two-dimensional TS wave. Through the non-linear interaction of this wave triad Λ-shaped vortices are formed in a staggered format that develops into turbulence.

Both transitional scenarios have been studied experimentally by Kachanov & Levchenko (1984). Direct numerical simulation (DNS) of K-type transition was performed by Rist & Fasel (1995). H-type transition was also reproduced computationally by Fasel *et al.* (1990) and Haertel & Kleiser (1993). These studies concentrated on the linear and non-linear stage of transition and gave little information on the secondary instabilities associated with the overshoot of the skin friction profile and the statistics of the boundary layer within each transitional regime and how such phenomena evolve with increasing Reynolds number.

The objective of this study is to explore the universality of downstream turbulence by numerically simulating K-type and H-type disturbances through DNS and comparing the resulting turbulent boundary layers against each other and the free-stream turbulence (FST) bypass transition of Wu & Moin (2010). The generated database is also available for validating the LES models applied to natural transition (see Sayadi & Moin 2011).

2. Computational domain

The code used to carry out these calculations is a compressible Navier-Stokes solver for ideal gas with Sutherland's law for viscosity. Conservation of kinetic energy in an inviscid limit is achieved by staggered collocation of velocities with respect to density and total energy in a structured curvilinear coordinate system using fourth order spatial

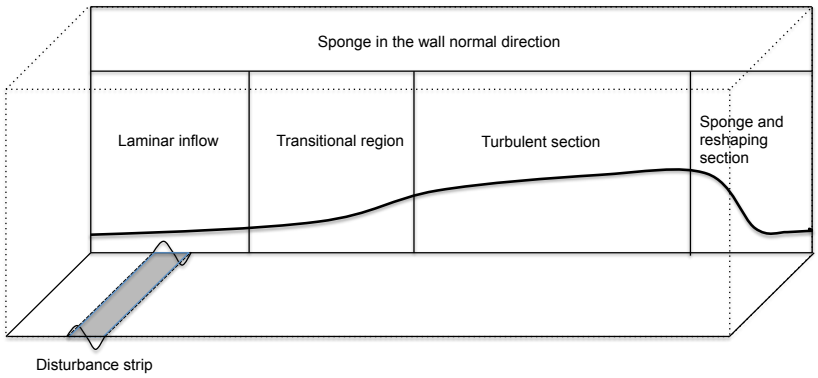

FIGURE 1. Computational domain.

	L_x	L_y	L_z	N_x	N_y	N_z	Δx^+	Δy^+_{min}	Δz^+	$Re_{\theta\max}$	λ_z
H-type	9.6	1.0	0.605	4096	550	512	10.684	0.414	6.720	1250	0.1514
K-type	8.599	0.92	0.606	4096	550	512	10.156	0.405	5.724	1410	0.1515

TABLE 1. Characteristics of the different grids.

derivatives in all three directions. Because of excessive resolution required close to the wall, all convective terms are treated implicitly in the near wall region, whereas an implicit A-stable second order scheme is applied to the viscous terms in the wall normal direction near the wall. All the remaining terms are advanced explicitly in time using an RK3 scheme.

The computational domain is shown in Figure 1. The non-dimensionalized molecular viscosity is 2×10^{-6} for both DNS calculations. The inlet Reynolds number based on the distance from the leading edge is $Re_x = 10^5$, and the characteristic length scale used for non-dimensionalization is based on the distance of the inlet station from the leading edge of the plate $x_0 = 1$. In the case of the H-type transition the dimensions of the computational domain are $1 \leq x/x_0 \leq 10.6$ in the streamwise direction, $0 \leq y/x_0 \leq 1$ in wall normal direction, and $0 \leq z/x_0 \leq 0.6055$ in the spanwise direction. This spanwise length is $5.2\delta_{99}$, where δ_{99} is the boundary layer thickness at $Re_\theta = 1250$. Spanwise two-point correlations also confirm that the width of the domain is adequate. The spanwise length is four times the wave length of the unstable oblique wave. The free stream velocity is constant and has been non-dimensionalized by the speed of sound in the free stream so that $Ma_\infty = 0.2$. The TS wave and subharmonic wave are introduced into the domain at the disturbance strip located upstream and extend from $x_1/x_0 = 1.655$ to $x_2/x_0 = 1.81$. The non-dimensionalized spanwise wavelength of the subharmonic wave is $\lambda_z/x_0 = 0.151367188$. These values are also shown in table 1.

For the K-type transition the inlet Reynolds number based on the distance from the leading edge is $Re_x = 10^5$. The dimensions of the computational domain are $1 \leq x/x_0 \leq 9.599$, $0 \leq y/x_0 \leq 0.92$, and $0 \leq z/x_0 \leq 0.606$. As a result the swise length is $5.18\delta_{99}$, where δ_{99} is the boundary layer thickness at $Re_\theta = 1400$. The disturbance strip is located upstream at $x_1/x_0 = 1.36$ and extends up to $x_2/x_0 = 1.56$. The non-dimensionalized spanwise wavelength of the subharmonic wave is $\lambda_z/x_0 = 0.1515$ as shown in Table 1.

For both transitional scenarios normal velocity at the location of disturbance strip

on the wall is modified in the form of the blowing and suction boundary condition of Huai *et al.* (1997) that models the effect of the vibrating ribbon in the experiment via a wall-normal velocity of the form:

$$v(x,z,t) = A_1 f(x)\sin(\omega t) + A_{1/2} f(x) g(z)\cos(\omega_0 t + \phi). \tag{2.1}$$

In the above equation, ω is the frequency of the two-dimensional TS wave. A_1 and $A_{1/2}$ are the disturbance amplitudes of first and subharmonic waves, and ϕ is the phase shift between the two. These values have been chosen such that the initial receptivity process matches the experiment of Kachanov & Levchenko (1984). From Fasel *et al.* (1990), we define $f(x)$ as

$$f(x) = 15.1875\xi^5 - 35.4375\xi^4 + 20.25\xi^3$$

$$\xi = \begin{cases} \frac{x-x_1}{x_m-x_1}, & \text{for} \quad x_1 \le x \le x_m \\ \frac{x_2-x}{x_2-x_m}, & \text{for} \quad x_m \le x \le x_2, \end{cases} \tag{2.2}$$

where $x_m = (x_1 + x_2)/2$ and $g(z) = \cos(2\pi z/\lambda_z)$. This method results in relatively clean TS waves downstream as all modes of disturbance except for the TS mode decay rapidly downstream. For the case of the H-type transition, because the oblique waves are of subharmonic nature, $\omega_0 = \omega/2$. $\phi = 0$, $A_1 = 0.002$, and $A_{1/2} = 0.0001$. For the case of the K-type transition the oblique waves have the same frequency as the two-dimensional wave, therefore $\omega_0 = \omega$. $\phi = 0$, $A_1 = 0.0075$, and $A_{1/2} = 0.0001$.

Periodic boundary conditions are used along the spanwise and streamwise directions. To account for the spatially growing boundary layer in a streamwise-periodic domain, we reshape the profile at the end of the domain into the similarity solution of a laminar compressible boundary layer at the inflow. This reshaping procedure is performed inside the sponge region (see Figure 1). Spalart & Watmuff (1993) used this method in a numerical simulation of a turbulent boundary layer. Inside all the sponges, which are situated at the top, inlet and outlet of the computational domain, the similarity solution of a compressible laminar boundary layer is prescribed.

Grid spacing for the H-type transition in the streamwise and spanwise directions was chosen to be $\Delta x/x_0 = 0.00235$ and $\Delta z/x_0 = 0.0014782$, respectively. Using the shear velocity at $Re_x = 6 \times 10^5$ where the overshoot of skin friction coefficient appears, this spacing can be expressed in wall normal units: $\Delta x^+ = 10.6839$ and $\Delta z^+ = 6.72038$. From previous calculations reported by Sayadi & Moin (2010) we can conclude that this transition scenario is more sensitive to spanwise than streamwise resolutions, therefore a finer spanwise resolution has been chosen here. The minimum grid spacing in the wall-normal direction for this transitional regime is $\Delta y = 9.10804 \times 10^{-5}$, equal to $\Delta y^+ = 0.41408$ in wall units. The maximum grid spacing is $\Delta y = 0.005273$.

For the K-type transition, the grid spacing in the streamwise and spanwise directions was chosen to be $\Delta x/x_0 = 0.0021$ and $\Delta z/x_0 = 0.0011836$. This flow transitions faster than the H-type transition such that the turbulent skin friction profile peaks at $Re_x = 3.2 \times 10^5$. As a result, the spacing in wall normal units based on shear velocity at this location is $\Delta x^+ = 10.1558$ and $\Delta z^+ = 5.724$. The smallest grid size in the wall normal direction for this transitional case is $\Delta y = 8.3794 \times 10^{-5}$, which in wall normal units is $\Delta y^+ = 0.40524$. The maximum grid size is $\Delta y = 0.004851$.

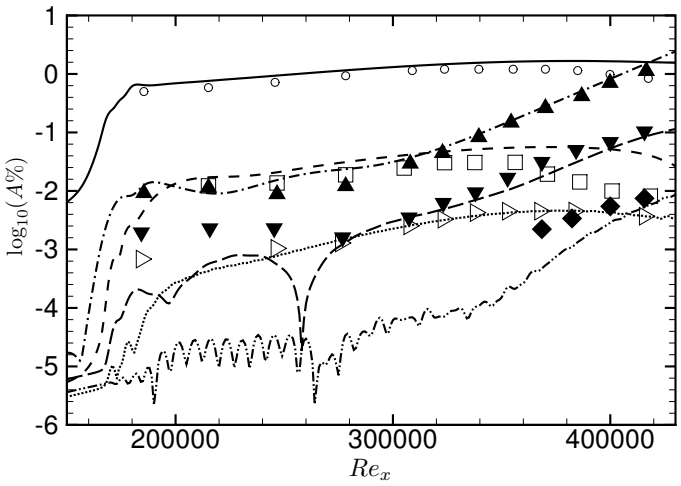

FIGURE 2. Percentage of disturbance amplitudes relative to free-stream velocity against Re_x, H-type transition. Numerical (lines) and experimental (symbols) results. —— and ○, (1,0); - - - and □, (2,0); ··· and ▷, (3,0); – · – and ▲, (1/2,1); – – – and ▼, (3/2,1); – ··– and ♦, (5/2,1).

3. Results

3.1. *Validation*

The evolution of disturbances is shown in Figures 2 and 3. Here the two- and three-dimensional disturbances are denoted in Fourier components (n, k) where n stands for the frequency of the disturbance as a multiple of the fundamental frequency and k is a multiple of the fundamental spanwise wavenumber. These results are from the Fourier analysis of two periods of the fundamental harmonic collected ten periods after the disturbance was initiated. The amplitudes of the H-type transition are compared with the experimental results of Kachanov & Levchenko (1984). The modes are calculated at a constant wall distance of $y/\delta = 0.26$, as in the experiment. There is good agreement between the amplitudes, calculated experimentally and numerically. The agreement is not as good at the end of the domain where the experimental results start to deviate from numerical values. Fasel *et al.* (1990) also saw the same behavior in their calculations. The discrepancy is attributed to the fact that only the first and second harmonics of the fundamental wave are introduced in the computations and therefore nonlinear interactions with higher disturbance harmonics are ignored.

The amplitudes of the K-type transition are compared with the numerical results reported by Rist & Fasel (1995) in Figure 3. There is good agreement between the two calculations. Based on these results H-type and K-type transition mechanisms are established.

3.2. *Visualization*

Figure 4 shows instantaneous snapshots of vortical structures inside the boundary layer for the K-type transition. The boundary layer is divided into six smaller sections and each section extends to approximately $\Delta x/x_0 = 1.05$ so that $\Delta Re_x = 1.05 \times 10^5$. Here we have chosen the iso-surfaces of the second invariant of the velocity gradient tensor, Q, to visualize the vortical structures in the flow. At $Re_x \simeq 2.6 \times 10^5$ the Λ-shaped

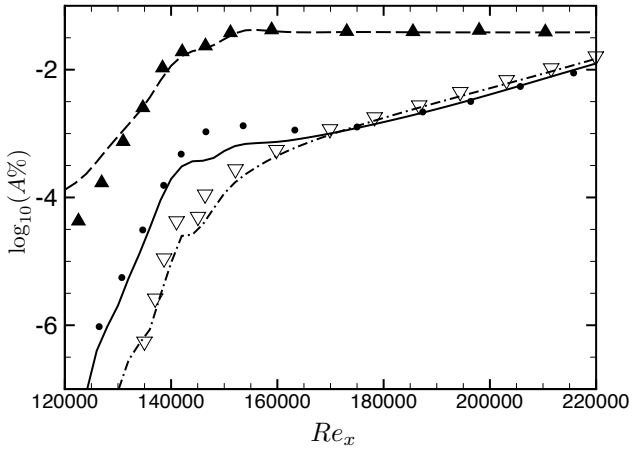

FIGURE 3. Percentage of disturbance amplitudes relative to free-stream velocity, K-type transition. Numerical (lines) and DNS of Rist & Fasel (1995) (symbols) results.– – – and ▲, (1,0); —— and •, $(0,1)$; – · – and ▽, (1,1).

vortices and the beginning of the secondary instability are seen. Four Λ-shaped vortices are identifiable. Note that the length of the spanwise direction is four times the wavelength of the unstable wave. The Λ-shaped vortices are also aligned in the downstream direction which is a characteristic of the K-type regime. These Λ-shaped vortices evolve into a packet of three hairpin vortices, which in turn lead to the formation of isolated turbulent regions at $3.2 \times 10^5 \leq Re_x \leq 3.6 \times 10^5$. Moving downstream, this region spreads and by $Re_x = 3.6 \times 10^5$ the boundary layer is fully populated across the spanwise direction by vortical structures. Iso-surfaces of Q are also plotted for the H-type transition in Figure 5. These are also instantaneous images where each section has the length $\Delta x/x_0 = 1.2$. Λ-shaped vortices are seen at $Re_x = 4.8{\times}10^5$. The Λ-shaped vortices are in staggered format as the flow develops downstream. This is a characteristic of the H-type transition. There are four Λ-shaped vortices at each spanwise location in the early transition stage. Note that the spanwise domain size is four times the wavelength of the most unstable wave. Four solitary Λ-shaped vortices finally develop into a packet of three hairpin vortices. This was also visible in the K-type transition case. In contrast to the K-type regime there are no localized turbulent spots in this case.

In contrast to the findings of Wu & Moin (2009) the dominance of the hairpin-like structures at the late turbulent stages is not as apparent. The regularity of the hairpin structures in the boundary layer of Wu & Moin (2009) could be the result of the periodically passing turbulent box. Because the box has a low decay rate, it interacts heavily with the boundary layer itself continuously triggering the same near-wall instabilities and causing the turbulent intensities to be non-zero away from the wall. This is not the case in the two natural transition cases studied here as the free stream is quiet and the transition is triggered by unstable modes introduced upstream. This will be explained further by examining the spanwise energy spectra in subsection 3.5.

3.3. *Integral parameters*

Variation of Reynolds number based on the momentum thickness, Re_θ, is plotted along the plate in Figure 6. The values based on Blasius profile and DNS of Wu & Moin (2010)

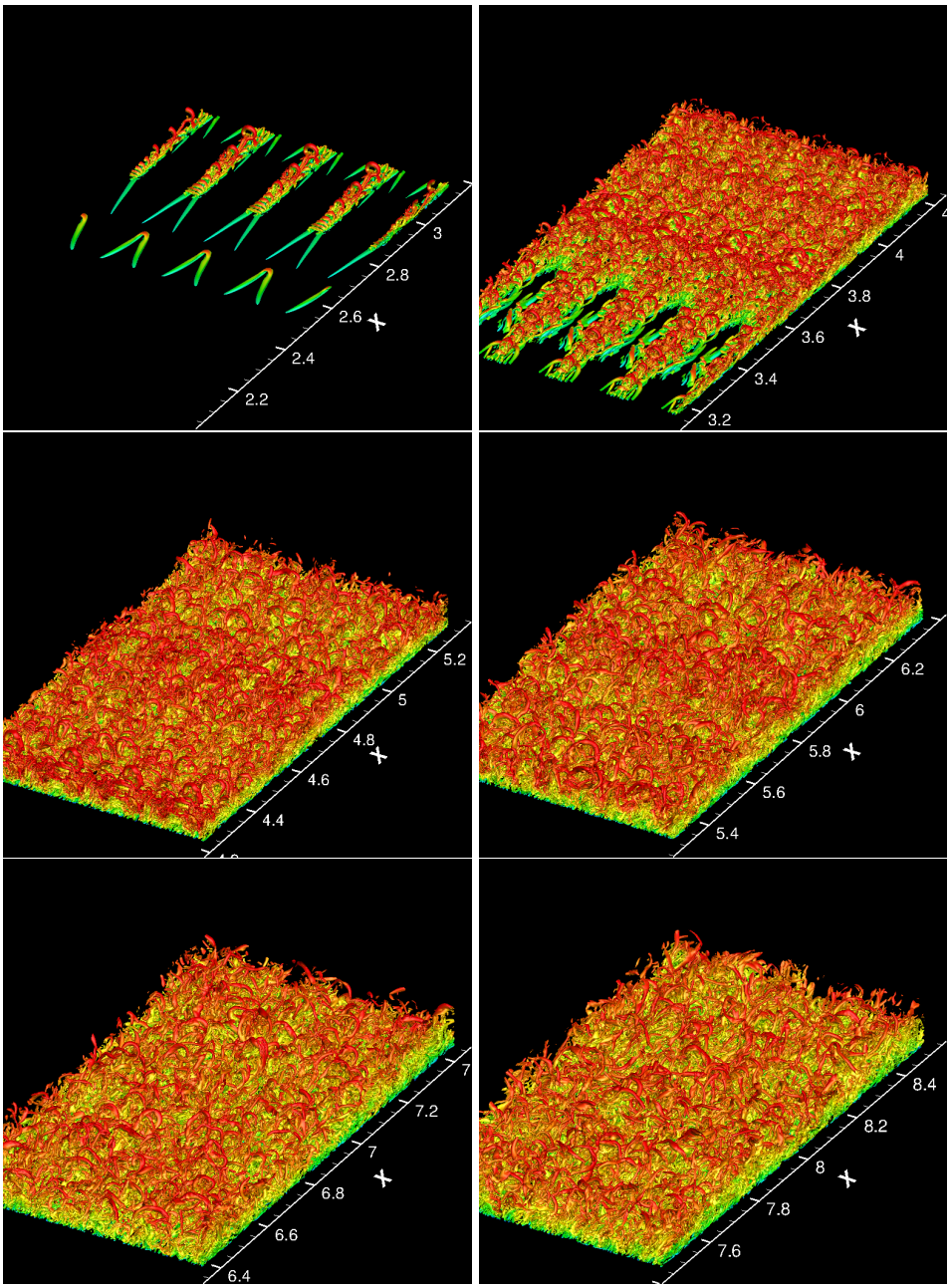

FIGURE 4. Iso-surfaces of second invariant of the velocity gradient tensor coloured by contours of streamwise velocity, for K-type transition scenario.

are also included. It can be seen that the boundary layer transitions fastest in the case of FST bypass of Wu & Moin (2010), and stays laminar longest in the case of the H-type transition. The highest Re_θ reached in the case of K-type transition is $Re_\theta = 1410$ at $x/x_0 = 8.3$ and the highest value for H-type transition is $Re_\theta = 1250$ at $x/x_0 = 9.03$.

Other integral parameters are the displacement thickness and shape factor. They are

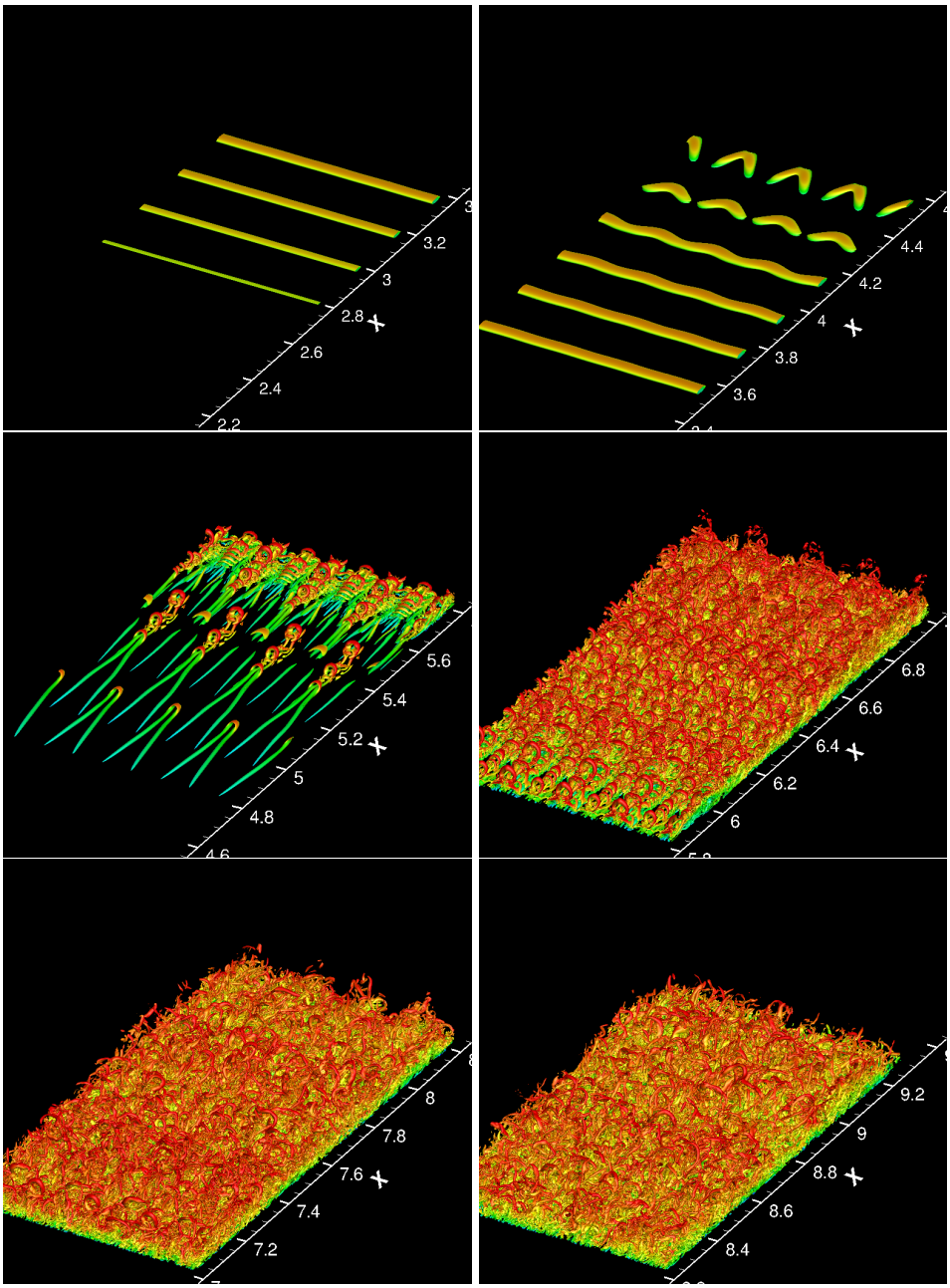

FIGURE 5. Iso-surfaces of second invariant of the velocity gradient tensor coloured by contours of streamwise velocity, for H-type transition scenario.

plotted in Figure 7 with respect to Re_θ. Transition is delayed in the H/K-type transition compared with the bypass transition.

The evolution of the skin friction with respect to Re_θ is shown in Figure 8. A gradual increase in the skin friction coefficient from laminar values to turbulent is seen for the case of the bypass transition. This is the region ($300 \leq Re_\theta \leq 500$) where random turbulent

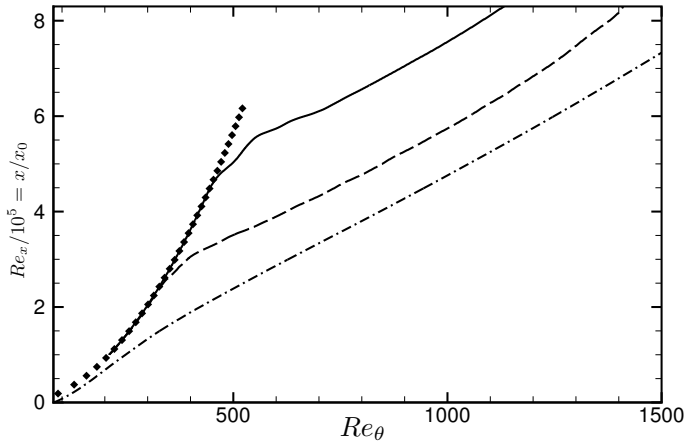

FIGURE 6. Variation of Re_θ along the plate: ——, H-type transition; – – –, K-type transition; – · –, FST bypass transition of Wu & Moin (2010); ♦, Blasius solution.

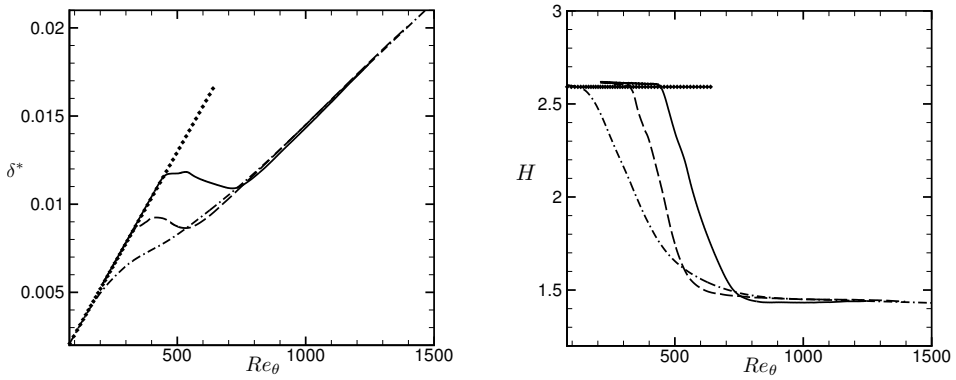

(a) Displacement thickness δ^* (b) Shape factor $H = \delta^*/\theta$

FIGURE 7. Displacement thickness, shape factor H: ——, H-type transition; – – –, K-type transition; – · –, FST bypass transition of Wu & Moin (2010); ♦, laminar.

spots appear in the domain leading to fully turbulent flow. Once the disturbances grow large enough the boundary layer diverges from the laminar solution and skin friction coefficient starts to rise. The skin friction coefficients in the turbulent stage are in good agreement.

3.4. *Mean and turbulent intensities*

In this section, we compare mean and turbulent statistics from the three turbulent boundary layers: the present K-type and H-type as well as the FST bypass transition from Wu & Moin (2010). Turbulence is initiated by different disturbances in each case, but the mean and turbulent statistics are largely the same as we now show. In Figure 9 the streamwise mean velocity profile is plotted in wall units. All profiles are in good agreement.

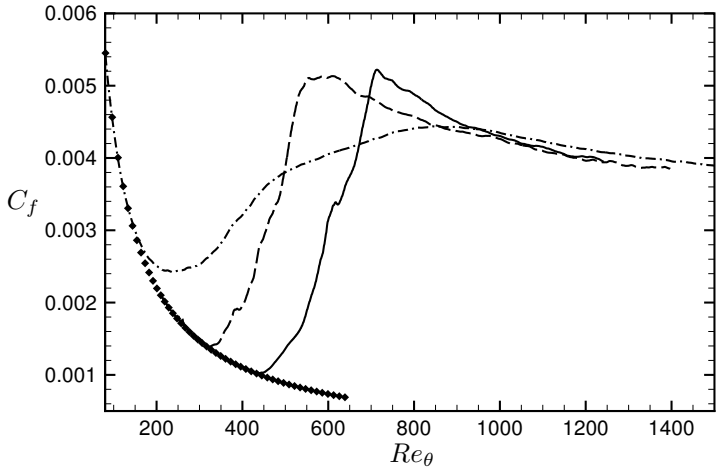

FIGURE 8. Variation of C_f along the plate vs. Re_θ: ——, H-type transition; − − −, K-type transition; − · −, FST bypass transition of Wu & Moin (2010); ♦, Laminar correlation.

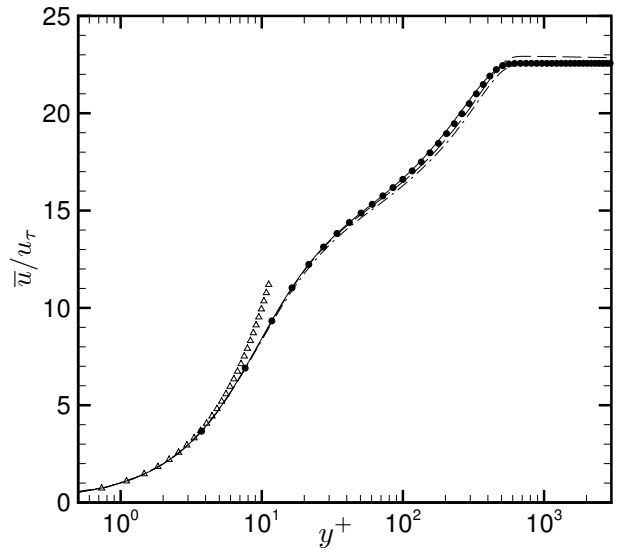

FIGURE 9. Mean velocity profiles: ——, H-type transition at $Re_\theta = 1250$; •, K-type transition at $Re_\theta = 1250$; − − −, K-type transition at $Re_\theta = 1410$; − · −, FST bypass of Wu & Moin (2010) at $Re_\theta = 1410$; △, $\overline{u}^+ = y^+$.

Turbulent intensities are plotted in Figure 10. The shear velocity, u_τ, used for normalization is calculated in the respective calculation. There is a good agreement between all profiles near the wall $y^+ \leq 100$ but the profiles do not collapse farther away from the wall. Away from the wall H-type and K-type transitions at $Re_\theta = 1250$ are in good

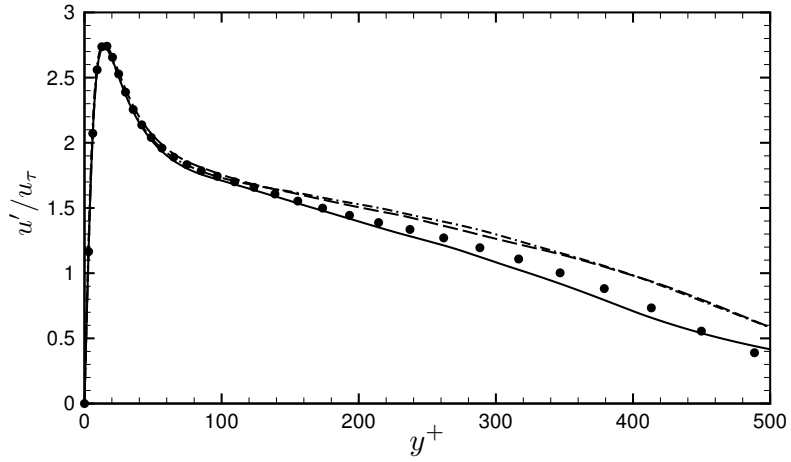

(a) Streamwise turbulent intensity

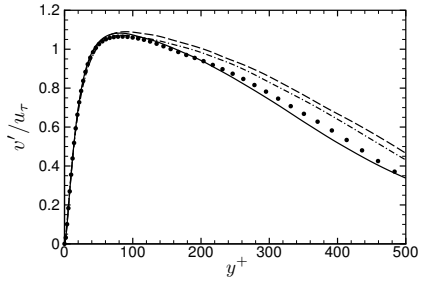

(b) Wall-normal turbulent intensity

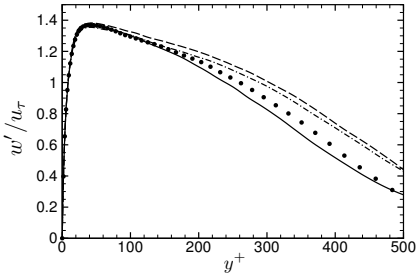

(c) Spanwise turbulent intensity

FIGURE 10. Turbulent intensities: ——, H-type transition $Re_\theta = 1250$; •, K-type $Re_\theta = 1250$; − − −, K-type $Re_\theta = 1410$; − · −, Wu & Moin (2010) $Re_\theta = 1410$.

agreement and lie below the profiles at $Re_\theta = 1410$. This suggests a Reynolds number effect in the shape of the turbulent intensity profiles farther away from the wall.

The Reynolds shear stress, $-\overline{u'v'}^+$, is plotted in Figure 11. The horizontal axis is normalized by inner layer variables. There appears to be a Reynolds number effect in the shape of the profile as we go farther from the wall. The profiles with same Re_θ are in better agreement.

3.5. *Energy spectra*

Time averaged spanwise energy spectra is plotted in Figure 12. The three plots correspond to energy specters at three different distances from the wall and streamwise location of $Re_\theta = 1200$. These distances in wall units are: $y^+ \simeq 5$, $y^+ \simeq 50$, and $y^+ \simeq 300$. Energy spectras of H-type transition have two distinct peaks corresponding to the harmonic and subharmonic wavelengths introduced upstream through the blowing and suction strip. The subharmonic disturbance can be seen in K-type energy spectra at $y^+ = 50$. The key difference between the current two controlled transition scenarios and the turbulence that results from free-stream disturbances applied by Wu & Moin (2009) is that

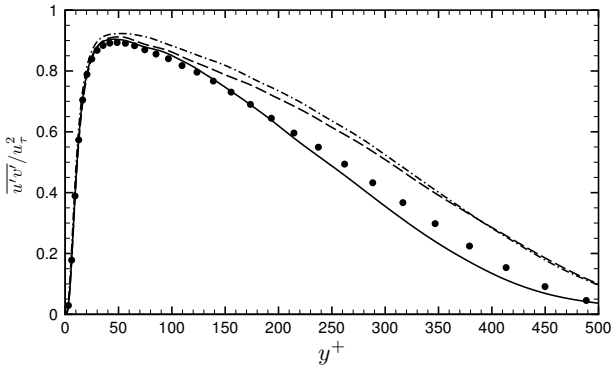

FIGURE 11. Reynolds shear stress: ——, H-type transition $Re_\theta = 1250$; •, K-type $Re_\theta = 1250$; − − −, K-type $Re_\theta = 1410$; − · −, Wu & Moin (2010) $Re_\theta = 1410$.

no "forest of hairpins" is found far downstream (at higher Reynolds numbers) in the H/K-type transition scenarios. The memory of these upstream disturbances fades away as non-modal interactions, which were originally very small but random perturbations to the disturbance strip forcing, become significant. As a result, the hairpin motions become less organized in the late-transitional regime whereupon a fully populated spanwise turbulent energy spectrum is established with no preference for modal interactions. Free-stream disturbances, on the other hand, are found to sustain a forest of hairpins (Wu & Moin 2009). FST persists far downstream providing a means to excite the same fundamental modes responsible for hairpin motions far into the fully turbulent flow. As a result, FST triggers these same mechanisms farther downstream maintaining coherent hairpin packets, whereas the convective instability in H/K-type is largely non-existent far downstream.

4. Conclusions

Transition to turbulence via spatially evolving secondary instabilities in compressible ($M_\infty = 0.2$), zero-pressure-gradient flat-plate boundary layers is numerically simulated for both the K-type and H-type disturbances. The objective of this work is to evaluate the universality of the breakdown process and coherent motion development between different routes through transition in wall-bounded shear flows. Each localized linear disturbance is amplified through weak non-linear instability that grows into Λ-vortices and then hairpin-shaped eddies with harmonic wavelength, which become less organized in the late-transitional regime once a fully populated spanwise turbulent energy spectrum is established. No forest of hairpins is found far downstream. In contrast, free-stream disturbances are able to sustain a forest of hairpins (Wu & Moin 2009). The key physical difference between the K/H-type transition and bypass transition produced by free-stream turbulence is that the FST persists far downstream providing a means to excite the same fundamental modes responsible for hairpin motion growth and development far into the fully turbulent flow. In effect, FST in such simulations triggers these same mechanisms farther downstream maintaining coherent hairpin packets, whereas the convective instability in the H/K-type is largely non-existent far downstream. Despite these differences, the mean statistics are quantitatively similar. As a result, incipient hairpin dynamics in

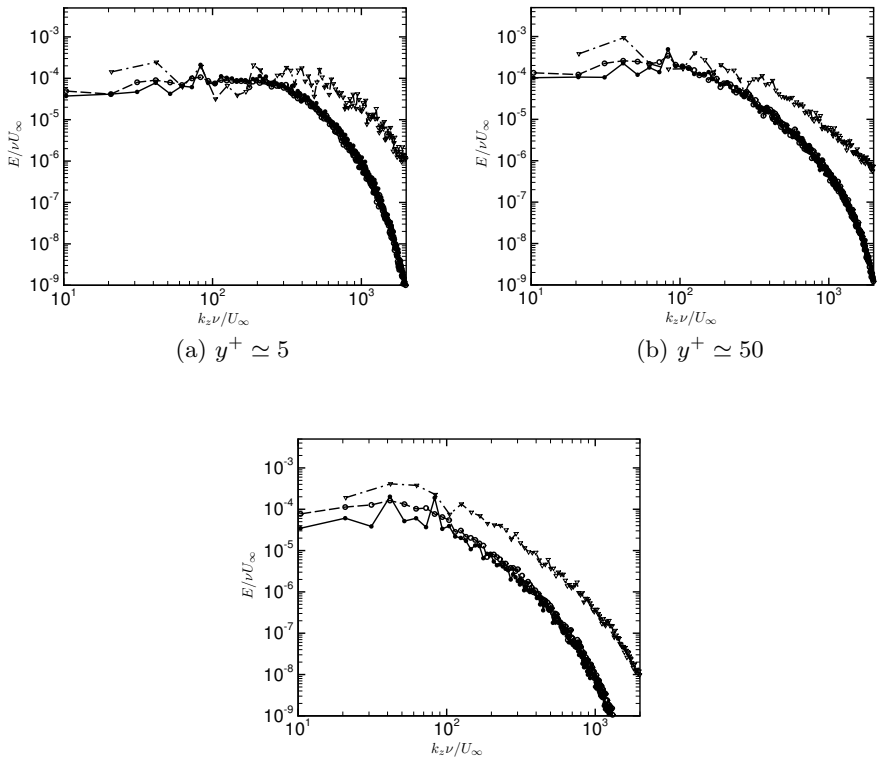

(a) $y^+ \simeq 5$ (b) $y^+ \simeq 50$

(c) $y^+ \simeq 300$

FIGURE 12. Spanwise energy spectra: ——, H-type transition; − − −, K-type; − · −, Wu & Moin (2010).

near-wall turbulence has merit as a physical modeling tool at higher Reynolds numbers (appearing directly in flows disturbances, such as FST, perturbing the near-wall layer thereby exciting the fundamental modes responsible for hairpin generation in the transitional regime). The mean near-wall turbulent statistics from DNS of K-type, H-type, and FST transition data are found to compare well with physical experiment and each other. Hence, the vortex regeneration mechanisms associated with hairpin-type coherent structures play a prominent role in near-wall turbulence dynamics and provide a foundation for modeling wall-bounded turbulent shear flows.

Acknowledgments

Computational support was provided by the Argonne Leadership Computing Facility at Argonne National Laboratory, supported by the Office of Science of the DOE, contract DE-AC02-06CH11357; DOE National Nuclear Security Administration, award number DE-FC52-08NA28613; and MRI-R2: Acquisition of a Hybrid CPU/GPU and Visualization Cluster for Multidisciplinary Studies in Transport Physics with Uncertainty Quantification, award number 0960306 funded under the American Recovery and Reinvestment Act of 2009 (Public Law 111-5). C.W. Hamman acknowledges support from a DOE Computational Science Graduate Fellowship, grant number DE-FG02-97ER25308.

REFERENCES

Fasel, H. F., Rist, U. & Konzelmann, U. 1990 Numerical investigation of three-dimensional development in boundary-layer transition. *AIAA* **28** (No. 1), 29–37.

Haertel, C. & Kleiser, L. 1993 Subharmonic transition to turbulence in channel flow. *Appleid Scientific Research* **51**, 43–47.

Herbert, T. 1988 Secondary instability of boundary layers. *Annu. Rev. Fluid Mech.* **20**, 487–526.

Huai, X., Juslin, R. D. & Piomelli, U. 1997 Large-eddy simulation of transition to turbulence in boundary layers. *Theoret. Comput. Fluid Dynam.* **9**, 149–163.

Kachanov, Y. S. & Levchenko, V. Y. 1984 The resonant interaction of disturbances at laminar-turbulent transition in a boundary layer. *J. Fluid Mech.* **138**, 209–247.

Klebanoff, P., K. D, T. & Sargent, L. M. 1962 The three-dimensional nature of boundary-layer instability. *J. Fluid Mech.* **12**, 1–34.

Rist, U. & Fasel, H. 1995 Direct numerical simulation of controlled transition in a flat-plate boundary layer. *J. Fluid Mech.* **298**, 211–248.

Sayadi, T. & Moin, P. 2010 A comparative study of subgrid scale models for the prediction of transition in turbulent boundary layers. *Center for Turbulence Research Annual Briefs* pp. 237–247.

Sayadi, T. & Moin, P. 2011 Predicting natural transition using large eddy simulation. *Center for Turbulence Research, Annual Research Briefs* .

Spalart, P. R. & Watmuff, J. H. 1993 Experimental and numerical study of a turbulent boundary layer with pressure gradients. *J. Fluid Mech.* **249**, 337–371.

Wu, X. & Moin, P. 2009 Direct numerical simulation of turbulence in a nominally zero-pressure-gradient flat-plate boundary layer. *J. Fluid Mech.* **630**, 5–41.

Wu, X. & Moin, P. 2010 Transitional and turbulent boundary layer with heat transfer. *Physics of Fluids* **22**, 85–105.